Journal of
Polymer Materials

Tech Science Press

https://doi.org/10.32604/jpm.2026.075384

ARTICLE

Multifunctional CEOS-DOPO-PDMS Modified Epoxy NP-GLIDE Coatings with Improved Combustion Behavior, Hydrophobicity, and Abrasion Resistance

Guoguan Wu[1,2], Baipei Liu[1,3], Dawei Jiang[1,2,*], Haorui Yu[1], Jiayu Fu[1,2], Chengze Yu[1], Hanbin Wang[1], Miaojun Xu[1,2,*], Zijian Wu[4] and Bin Li[1,2,*]

[1]College of Chemistry, Chemical Engineering and Resource Utilization, Northeast Forestry University, Harbin, China
[2]Heilongjiang Key Laboratory of Molecular Design and Preparation of Flame Retarded Materials, Northeast Forestry University, Harbin, China
[3]Aulin College, Northeast Forestry University, Harbin, China
[4]Department of Material Science and Technology, Harbin University of Science and Technology, Harbin, China

*Corresponding Authors: Dawei Jiang. Email: daweijiang@nefu.edu.cn; Miaojun Xu. Email: xumiaojun@nefu.edu.cn; Bin Li. Email: libinzh62@163.com

Received: 30 October 2025; Accepted: 16 January 2026; Published: 03 April 2026

ABSTRACT: Epoxy resins are extensively employed in the construction, electronics, automotive, and aerospace industries owing to their outstanding mechanical strength, chemical resistance, and electrical insulation. However, their intrinsic flammability, poor wear resistance, and hydrophilicity significantly restrict broader applications. To address these challenges, a novel multifunctional coating (CEOS-DOPO-PDMS) has been designed and fabricated via an NP-GLIDE approach. The system integrates 9,10-dihydro-9-oxa-10-phosphaphenanthrene-10-oxide (DOPO) as a reactive phosphorus-based flame retardant, epoxy-terminated polydimethylsiloxane (EP-PDMS) as a hydrophobic segment, and cycloaliphatic epoxy-functionalized oligosiloxanes (CEOS) as a cross-linking co-reactant. The resulting CEOS-DOPO-PDMS hybrid precursor was blended with bisphenol A diglycidyl ether (DGEBA) in N-methyl-2-pyrrolidone (NMP) and subsequently cured to form epoxy-based NP-GLIDE coatings. The optimized coating exhibits superior integrated performance, including high hydrophobicity (water contact angle up to 109.6°), outstanding abrasion resistance (5H pencil hardness), and excellent flame retardancy (resisting combustion at 500°C for 30 s). These enhancements originate from the cooperative effects of the Si-O-Si framework, low-surface-energy PDMS chains, and phosphorus-containing DOPO moieties, which together provide stable thermal protection, surface roughness-induced hydrophobicity, and durable mechanical integrity. An effective strategy for constructing multifunctional epoxy-based coatings with simultaneously enhanced flame retardancy, wear resistance, and water repellency is presented. The CEOS-DOPO-PDMS system holds great promise for advanced protective applications in construction, transportation, and aerospace engineering.

KEYWORDS: NP-GLIDE; epoxy resin; flame retardant; abrasion resistance; hydrophobic coating

1 Introduction

Epoxy resin is an essential class of thermosetting polymers characterized by excellent mechanical strength, strong adhesion, chemical resistance, and electrical insulation properties [1]. Owing to these versatile properties, epoxy resins are extensively used in high-performance applications such as coatings [2,3], adhesives [4,5], electronic encapsulation [6,7], and structural composites [8–10]. The growing demand for

durable and multifunctional materials in industrial and technological sectors has accelerated the development of epoxy-based systems. However, pristine epoxy resins are inherently flammable, hydrophilic, and prone to wear damage, which greatly limits their long-term stability and application in harsh environments. Therefore, improving the flame retardancy, hydrophobicity, and abrasion resistance of epoxy resins has become an urgent focus [11,12].

Among various modification strategies, the incorporation of flame retardants has proven to be an effective approach to reduce the flammability of epoxy systems [13]. Compared to halogen-containing compounds, phosphorus-based flame retardants have gained considerable attention owing to their high efficiency and environmental compatibility [14,15]. In particular, 9,10-dihydro-9-oxa-10-phosphaphenanthrene-10-oxide (DOPO) and its derivatives have demonstrated remarkable potential in enhancing the flame resistance of epoxy networks due to their high reactivity and good thermal stability [16,17]. During the thermal degradation of the polymer matrix, DOPO releases PO radicals, some of which escape reaction with matrix components and enter the gas phase, where they efficiently scavenge combustion-propagating radicals [18,19]. It should be clearly stated that only DOPO derivatives incorporating molecular structures active in the condensed phase, or those that alter DOPO's mode of action, can enable protective layer formation during combustion. Given these considerations, combining DOPO with siloxanes has proven to be an effective strategy for enhancing flame retardancy through synergistic action, as supported by numerous studies [20,21]. Specifically, during combustion, siloxanes decompose to form a dense silica-based protective layer covering the material surface, blocking the transfer of heat and combustible gases. Meanwhile, DOPO releases PO radicals in the gas phase to eliminate active radicals, suppressing the combustion chain reaction. This dual-mode synergy (gas-phase radical eliminating combined with condensed-phase barrier formation) not only improves flame retardant efficiency but also enhances char layer quality, thereby overcoming the limitations of DOPO alone. DOPO units have been successfully introduced into epoxy systems through chemical grafting or reactive curing, achieving significant improvements in flame retardancy and thermal stability [22,23]. Nevertheless, these DOPO-modified epoxy resins often suffer from insufficient hydrophobicity and poor wear resistance, which continue to hinder their practical application as protective coatings.

The NP-GLIDE (Nanoparticle Surface Functionalization) technology provides an innovative solution for fabricating durable hydrophobic coatings [24,25]. This approach incorporates polydimethylsiloxane (PDMS)-based modifiers into polymer matrices, leading the formation of surface-enriched low-energy domains that enhance water repellency and abrasion resistance without compromising bulk mechanical properties [26]. PDMS-functionalized coatings exhibit superior water- and oil-repellency, transparency, and durability [27–29]. When applied to epoxy resins [30,31], NP-GLIDE technology can effectively reduce surface hydrophilicity and mechanical degradation caused by environmental exposure. This approach thus provides a promising platform for multifunctional coating design.

Building upon these concepts, a new design strategy that integrates flame retardancy, hydrophobicity, and mechanical robustness within a single epoxy-based NP-GLIDE coating system has been developed. A hybrid precursor was synthesized by combining DOPO as a reactive phosphorus-containing flame retardant, epoxy-terminated PDMS (EP-PDMS) as a hydrophobic segment, and cycloaliphatic epoxy-functionalized oligosiloxanes (CEOS) as a co-crosslinking agent [32]. The resulting CEOS-DOPO-PDMS hybrid was incorporated into bisphenol A diglycidyl ether (DGEBA) to form a multifunctional coating with good performance characteristics.

The synthesis, structure, and comprehensive properties of the CEOS-DOPO-PDMS-modified epoxy NP-GLIDE coating (Fig. 1) have been investigated. Through detailed characterization including FTIR analysis, surface morphology observation, hydrophobicity testing, abrasion evaluation, and flame-retardancy

assessment, the relationships between composition, microstructure, and macroscopic performance have been clarified. This study provides new insights into the molecular design of multifunctional epoxy coatings and offers a feasible pathway toward next-generation protective materials for applications in construction, electronics, and aerospace engineering.

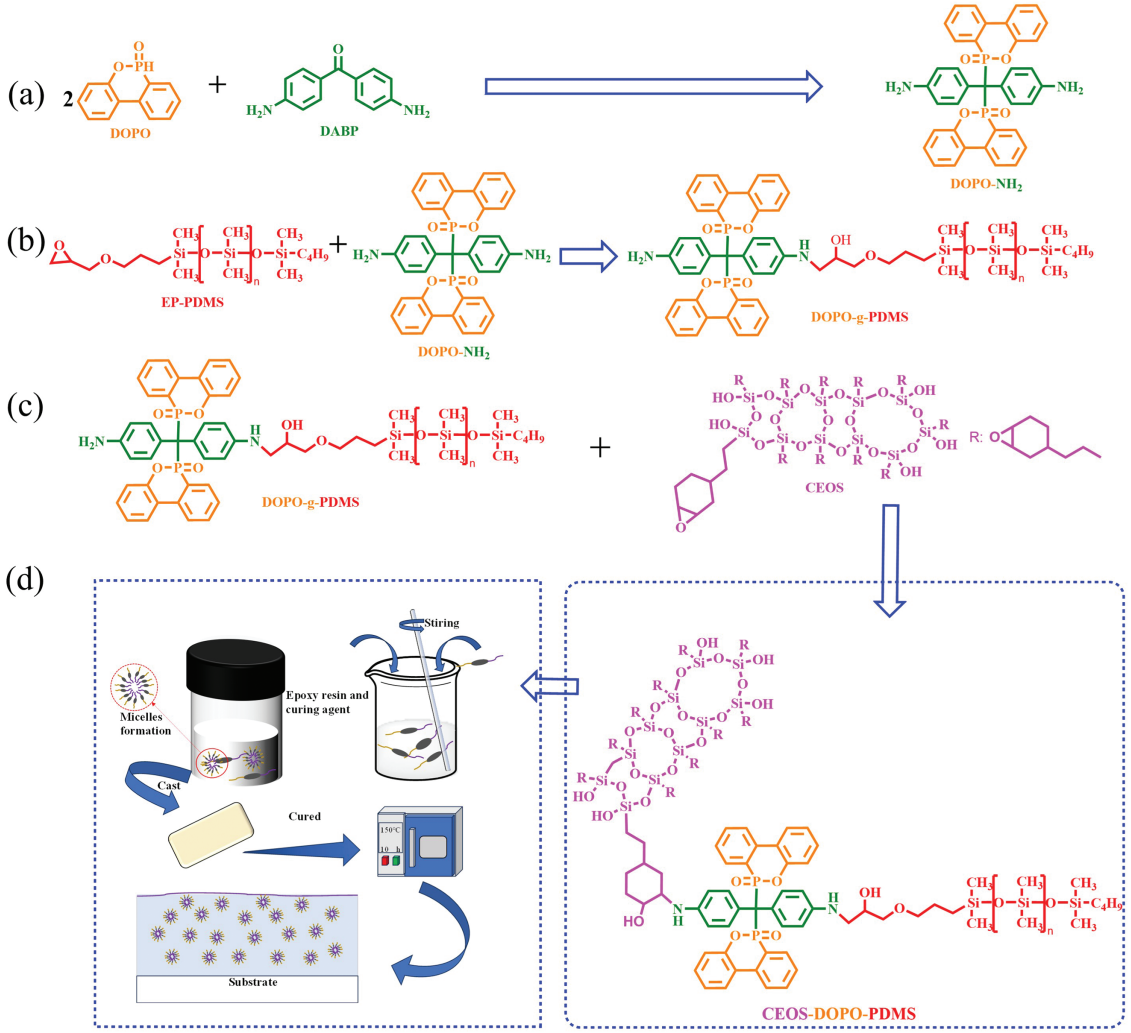

Figure 1: (**a**) Synthesis route of DOPO–NH_2, (**b**) one possible epoxy-amine addition route for the formation of DOPO-g-PDMS, (**c**) one possible reaction route for the formation of CEOS-DOPO-PDMS, (**d**) schematic illustration of preparation procedure of the epoxy-based NP-GLIDE coatings.

2 Materials and Methods

2.1 Materials

9,10-Dihydro-9-oxa-10-phosphaphenanthrene-10-oxide (DOPO, 97%) and [2-(3,4-epoxycyclohexyl) ethyl]trimethoxysilane (ECTS, 99%) were purchased from Shanghai Macklin Biochemical Technology Co., Ltd. Bisphenol A diglycidyl ether (DGEBA, 85 wt%, epoxy equivalent weight, EEW = 188 ± 2 $g{\cdot}eq^{-1}$) and 4,4′-diaminobenzophenone (DABP, 99%) were obtained from Shanghai Macklin Biochemical Technology Co., Ltd. and Shanghai Bide Pharmaceutical Technology Co., Ltd., respectively. Toluene, chloroform, tetrahydrofuran (THF), methanol, ethyl acetate, acetonitrile, and N-methyl-2-pyrrolidone (NMP, 99%) were

of analytical grade and supplied by Shanghai Aladdin Biochemical Technology Co., Ltd. Epoxy-terminated polydimethylsiloxane (EP-PDMS, 99 wt%, number-average molecular weight, Mn ≈ 5000 g·mol^{-1}, average siloxane chain length ≈ 70 repeat units) and polyetheramine Jeffamine D230 (Mn ≈ 230 g·mol^{-1}, amine hydrogen equivalent weight, AHEW = 60 ± 1 g·eq^{-1}) were purchased from Shanghai Sigma-Aldrich Trading Co., Ltd. Aqueous ammonia ($NH_3 \cdot H_2O$, 25%) and sodium hydroxide (NaOH) were obtained from Sinopharm Chemical Reagent Co., Ltd. All reagents were used as received without further purification.

2.2 Synthesis of Functional Precursors

2.2.1 Preparation of DOPO-NH_2

Following the procedures reported by Wu and Wang et al. [33,34], DOPO–NH_2 was synthesized via a condensation reaction between DOPO and DABP. DOPO (6.49 g, 0.03 mol) and DABP (1.06 g, 0.005 mol) were added into a three-neck flask under nitrogen protection and heated to 180°C for 4 h. The solid gradually melted into a viscous liquid. After cooling to 110°C, toluene (10 mL) was added dropwise to induce precipitation. The crude product was filtered, washed with THF and methanol (10 mL each), and vacuum-dried at 60°C to obtain a white solid (DOPO–NH_2) (Fig. 1a).

2.2.2 Grafting of DOPO onto PDMS (DOPO-g-PDMS)

DOPO-NH_2 (1.0 g) and EP-PDMS (1.2 g) were dissolved in chloroform (10 mL), followed by addition of triethylamine (2 mL) as a catalyst [30]. The mixture was transferred to a Schlenk flask, purged with nitrogen, and heated at 60°C for 48 h under stirring. After the reaction, the solvent and triethylamine were removed by rotary evaporation under reduced pressure, and the residue was vacuum-dried at 60°C for 4 h to yield DOPO-g-PDMS as a white solid (Fig. 1b). As illustrated in Fig. 1b, the structure is proposed as one plausible and likely predominant grafting outcome rather than a uniquely defined molecular structure. Considering the excess of DOPO-NH_2 and the limited number of reactive sites on PDMS, extensive crosslinking is unlikely, and mono-grafted species are expected to dominate.

2.2.3 Synthesis of Cycloaliphatic Epoxy-Functionalized Oligosiloxane (CEOS)

CEOS was synthesized via a sol–gel condensation route [35]. ECTS (4.0 g, 8.1 mmol), aqueous ammonia (0.44 mL, 2.0 mol·L^{-1}), and NaOH solution (10 μL, 1.0 mol·L^{-1}) were mixed in a round-bottom flask and stirred at 80°C for 4 h. After the reaction, methanol was removed by rotary evaporation to obtain a light-yellow viscous liquid corresponding to CEOS.

2.2.4 Fabrication of CEOS-DOPO-PDMS Hybrid Precursor

To prepare the hybrid precursor [36], CEOS (1.0 g), ethyl acetate (2 mL), and DOPO-g-PDMS (55 mg) were introduced into a three-neck flask. The mixture was refluxed at 85°C for 1.5 h under nitrogen. After cooling to room temperature, the product was precipitated in acetonitrile (14 mL) and centrifuged at 6000 rpm for 10 min. The resulting solid was dried to yield the CEOS-DOPO-PDMS hybrid precursor (Fig. 1c).

2.3 Preparation of Epoxy-Based NP-GLIDE Coatings

The epoxy-based NP-GLIDE coatings were prepared using a cast-coating technique on clean glass substrates (50 mm × 50 mm, area: 25 cm^2). For each formulation, CEOS-DOPO-PDMS (0, 5, or 20 mg) was first dispersed in N-methyl-2-pyrrolidone (NMP, 5 mL), followed by the addition of DGEBA (100 mg) and Jeffamine D230 (38 mg) [37,38]. After thorough stirring to obtain a uniform mixture, the suspensions were

cast onto the substrates and cured at 150°C for 2.5 h (Fig. 1d), yielding samples I (0 mg), II (5 mg), and III (20 mg). During curing, NMP was completely evaporated, therefore, the final film thickness was determined solely by the solid mass in each formulation, consisting of DGEBA (100 mg), Jeffamine D230 (38 mg), and CEOS-DOPO-PDMS (0, 5, or 20 mg), corresponding to a total solid content of 138–158 mg. Using the typical density of cured epoxy (~1.2 g·cm^{-3}), the theoretical thickness h was estimated according to:

$$h = \frac{m}{A\rho}$$

where m is the mass of the cured solid (mg), A is the coating area (25 cm^2), and ρ is the density of the cured epoxy network (~1.2 g·cm^{-3}). Substituting the above values yields an estimated thickness of approximately 46–53 μm. Since the casting volume and total solid loading were held constant for all formulations, the coating thickness is expected to remain uniform across samples I–III.

2.4 Characterization

2.4.1 FT-IR Analysis

Fourier transform infrared (FT-IR) spectra were recorded on a PerkinElmer Spectrum 400 spectrometer in the range of 4000–450 cm^{-1} with a resolution of 4 cm^{-1}. Samples were prepared as KBr pellets by thoroughly mixing the powdered materials with spectroscopic-grade KBr.

2.4.2 Surface Morphology and Hydrophobicity Evaluation

Surface topography of the coatings was observed under an optical microscope (TH4-200) at 60× and 100× magnifications. Water contact angles were measured using a Krüss DSA-100S contact angle analyzer. Each coating was tested in triplicate, and the mean value was reported to evaluate surface hydrophobicity.

Density functional theory calculations were performed using Gaussian 16 [39]. All compound molecules were structurally optimized using the B3LYP functional [40,41], with the standard 6-311^{++}G(d,p) basis set [42,43] applied to all atoms.

2.4.3 Abrasion Resistance Testing

Wear resistance was evaluated via pencil hardness and steel-wool abrasion tests. Pencils ranging from 1H to 6H were used to scratch the coating surfaces under consistent force, followed by microscopic examination (20×). Additional testing involved repeatedly rubbing with cotton swabs and steel wool pads for varying numbers of times. The degree of visible damage was used to compare abrasion resistance among samples. The scratch resistance of the NP-GLIDE coatings was evaluated according to the ASTM D3363 pencil hardness test. Pencils with hardness grades from H to 6H were sharpened and conditioned to obtain smooth, flat circular lead tips. Each pencil was mounted on an Elcometer 501 Hardness Tester, which positioned the pencil at a 45° angle and applied a constant downward force of 7.5 N. Beginning with the hardest pencil (6H), the tester was pushed forward across the coating surface. When a visible scratch or wear trace was observed, the test was repeated with the next softer pencil. This procedure continued until a pencil grade produced no visible mark. The scratch resistance was defined as the highest pencil hardness that did not damage the coating surface.

Abrasion resistance against cotton swabs and steel wool was measured using a Taber Abrasion Tester following the ASTM D4060 standard. The coated samples were fixed on a horizontal platform, and the abrasive media were installed in the test arms to ensure uniform surface contact. Cotton swab abrasion tests were performed for 10 rubbing cycles under a vertical load of 100 g. Steel wool abrasion tests were conducted

for 10 and 50 rubbing cycles under a vertical load of 500 g. After testing, the coatings were evaluated based on the degree of surface wear, including gloss reduction, visible scratching, and material loss.

2.4.4 Combustion Behavior Analysis

Combustion behavior was examined using a butane torch positioned 15 cm from the surface of the coating (with a thickness of approximately 46–53 μm) for 30 s. The surface morphology and temperature evolution during combustion were monitored using a Uti32 infrared thermal imager (Uni-Trend Technology Co., Ltd., China). The extent of carbonization and residual char morphology were analyzed to assess flame-retardant efficiency.

3 Results and Discussion

3.1 FT-IR Analysis of Synthesized Precursors and Epoxy-Based NP-GLIDE Coatings

Fourier transform infrared (FT-IR) spectroscopy was employed to verify the successful synthesis of the functional intermediates and to confirm the structural evolution during coating formation. Fig. 2a–c presents the FT-IR spectra of DOPO–NH_2, CEOS–DOPO-PDMS, and the final epoxy-based NP-GLIDE coating, together with their corresponding raw materials.

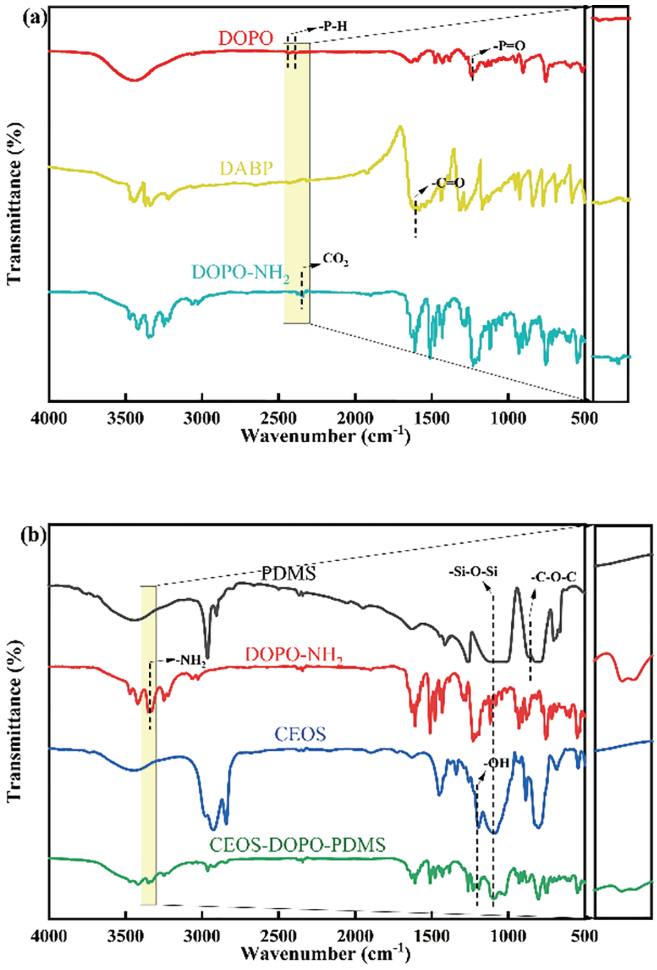

Figure 2: (Continued)

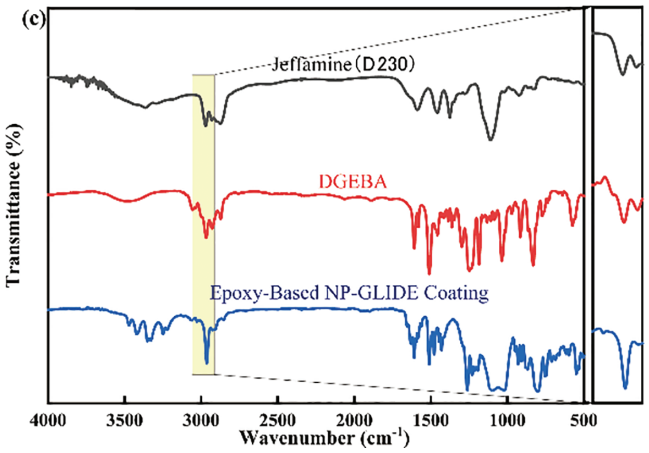

Figure 2: (**a**) Infrared spectrum of DOPO-NH_2, (**b**) Infrared spectrum of CEOS-DOPO-PDMS, (**c**) Infrared spectrum of Epoxy-Based NP-GLIDE Coatings.

3.1.1 Structural Verification of DOPO–NH_2

As shown in Fig. 2a, the pristine DOPO exhibits a characteristic P–H stretching vibration at 2390 cm^{-1}. The band corresponding to P–H vibrations decreases significantly in intensity after reaction with 4,4′-diaminobenzophenone (DABP), indicating the consumption of a large fraction of P–H bonds in DOPO and the formation of P–N linkages in DOPO–NH_2. Concurrently, a broad and intense N–H stretching vibration appears near 3400 cm^{-1}, accompanied by enhanced aromatic C=C absorptions in the 1600–1500 cm^{-1} region. Notably, no characteristic absorption peak of the C=O group (derived from DABP) is detected in the product. These spectral changes together strongly confirm the successful synthesis of the amino-functionalized DOPO–NH_2, and imply that any unreacted DOPO or DABP, if present, is in negligible amounts.

3.1.2 Formation of CEOS–DOPO-PDMS Hybrid Precursor

The FT-IR spectrum of CEOS–DOPO-PDMS (Fig. 2b) reveals distinct characteristic absorptions from both siloxane and phosphorus-containing moieties, demonstrating the successful integration of the PDMS and DOPO segments into the CEOS framework. The stretching vibration of –CH_3 groups from PDMS is clearly observed at 2970 cm^{-1}, while Si–O–Si asymmetric stretching appears at approximately 1100 cm^{-1}. The amino-related N–H band near 3400 cm^{-1} observed in DOPO–NH_2 markedly decreases in intensity and broadens in CEOS–DOPO-PDMS, confirming the consumption of amino groups during the condensation reaction with CEOS. Furthermore, compared with CEOS, the CEOS–DOPO-PDMS spectrum exhibits a clear reduction in the epoxy-ring absorption band at ~910 cm^{-1}, together with a slight increase in the –OH-related bands near 1200 cm^{-1}. These changes are consistent with partial epoxy ring-opening during the condensation process, accompanied by the formation of hydroxyl groups. Because the characteristic absorptions of Si–O–Si dominate the region of 1000–1130 cm^{-1} and strongly overlap with signals from any possible ring-opened intermediates, the spectra do not allow specific identification of individual newly formed Si-containing linkages. Nevertheless, the observed decrease in epoxy content and the intensified Si–O–Si envelope collectively indicate that progressive condensation and network development occurred during the conversion from CEOS to CEOS–DOPO-PDMS.

These spectroscopic evolutions validate the formation of a chemically bonded hybrid structure containing phosphorus, silicon, and PDMS segments, which is essential for imparting flame retardancy, flexibility, and hydrophobicity to the final coating. The FT-IR spectral evolution provides supportive evidence for

the occurrence of the grafting reaction, although the exact substitution pattern cannot be unambiguously determined based on FT-IR analysis alone.

3.1.3 Structural Characteristics of Epoxy-Based NP-GLIDE Coatings

The FT-IR spectrum of the cured epoxy-based NP-GLIDE coating shows prominent absorptions at 2970 cm^{-1} (–CH_3 stretching) and 1100 cm^{-1} (Si–O–Si stretching), together with a broad band near 3400 cm^{-1} attributed to residual hydroxyl and N–H groups formed during curing (Fig. 2c). The disappearance of the characteristic epoxy ring band at 910 cm^{-1} and the appearance of new C–O–C stretching peaks around 1250 cm^{-1} indicate complete cross-linking between DGEBA and Jeffamine D230. Moreover, the persistence of Si–O–Si and –CH_3 vibrations confirms that the low-surface-energy PDMS segments are retained on the coating surface, contributing to hydrophobicity and lubricity.

Overall, the FT-IR results provide clear spectral evidence of successful stepwise synthesis from DOPO-functionalization to siloxane hybridization and epoxy network formation. The coexistence of P–O, Si–O–Si, and C–O–C structures within the final coating verifies the molecular integration of flame-retardant, siloxane, and hydrophobic components. This hybridized architecture forms the chemical basis for the superior thermal stability, surface hydrophobicity, and mechanical robustness of the CEOS-DOPO-PDMS-modified NP-GLIDE epoxy coatings.

3.2 Surface Morphology and Performance Analysis

3.2.1 Surface Morphology Observation

The surface morphologies of epoxy-based NP-GLIDE coatings with different CEOS–DOPO–PDMS contents were examined under optical microscopy at magnifications of 60× and 100×, as shown in Fig. 3. The unmodified epoxy coating (CEOS–DOPO–PDMS:DGEBA = 0:100) exhibited a relatively smooth and dense surface, typical of conventional cross-linked epoxy networks (Fig. 3a,b). In contrast, the coatings containing CEOS–DOPO–PDMS displayed markedly rougher surfaces with micro-scale protrusions and uneven topography (Fig. 3c–f). This surface evolution can be attributed to the incorporation of PDMS segments, which migrate toward the air–polymer interface during curing due to their low surface energy. Additionally, the volatilization of NMP solvent induces micro-phase separation and localized void formation, further enhancing surface roughness. Such hierarchical structures are beneficial for forming air-trapping microtextures that enhance hydrophobicity and abrasion resistance.

3.2.2 Hydrophobicity Evaluation

Water contact angle measurements were conducted to quantify the surface wettability of coatings with varying CEOS–DOPO–PDMS content (Fig. 4). The unmodified epoxy coating exhibited contact angles of 39.7°–64.5°, confirming its hydrophilic nature. In contrast, coatings containing CEOS–DOPO–PDMS exhibited significantly increased contact angles, reaching 107.8°–109.6° for the 5:100 and 105.1°–109.4° for the 20:100 formulations. The nearly constant high contact angles across both compositions suggest that once a sufficient concentration of PDMS segments is present, the surface becomes saturated with low-surface-energy Si–CH_3 groups, producing stable hydrophobic behavior independent of additional loading [44,45]. The enhanced hydrophobicity is primarily attributed to two synergistic factors: (i) enrichment of PDMS chains at the surface, and (ii) increased micro/nano roughness generated by solvent-induced phase separation. The formation of a Cassie–Baxter wetting regime enables water droplets to rest on trapped air pockets, explaining the pronounced water repellency observed.

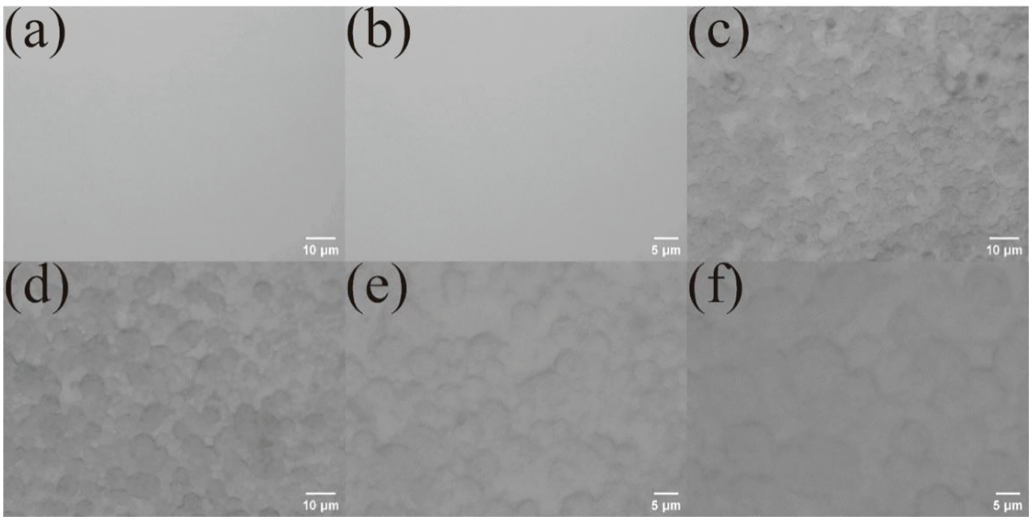

Figure 3: Optical microscopy images of epoxy-based NP-GLIDE coatings containing three different CEOS-DOPO-PDMS ratios at varying magnifications, (**a**,**c**,**d**) coatings with CEOS-DOPO-PDMS to DGEBA mass ratios of 0:100, 5:100, and 20:100, respectively, observed under 100× magnification, (**b**,**e**,**f**) corresponding coatings observed under 60× magnification for the same respective ratios.

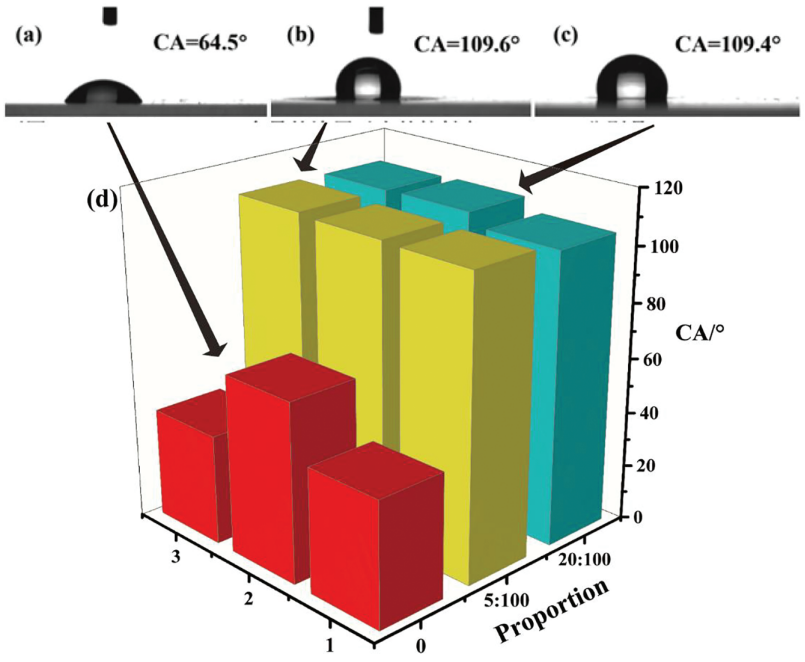

Figure 4: (**a**–**c**) The contact-angle images of coatings with CEOS-DOPO-PDMS:DGEBA mass ratios of 0:100, 5:100, and 20:100, and (**d**) contact angle measurements of coating combinations with varying compositions.

Density functional theory (DFT) calculations were carried out for the DOPO-NH_2-PDMS structure to obtain its optimized geometry and vibrational frequencies. The calculations were performed using GaussView with the DFT-B3LYP method and the 6-31G^{+++} basis set. Electrostatic potential surface (EPS)

analyses were subsequently conducted. Fig. 5a,b shows the minimum-energy structures of DOPO-NH_2-PDMS and H_2O, respectively, while Fig. 5c,d presents their corresponding EPS maps. In these maps, red regions represent electron-rich areas, whereas blue regions indicate electron-deficient regions.

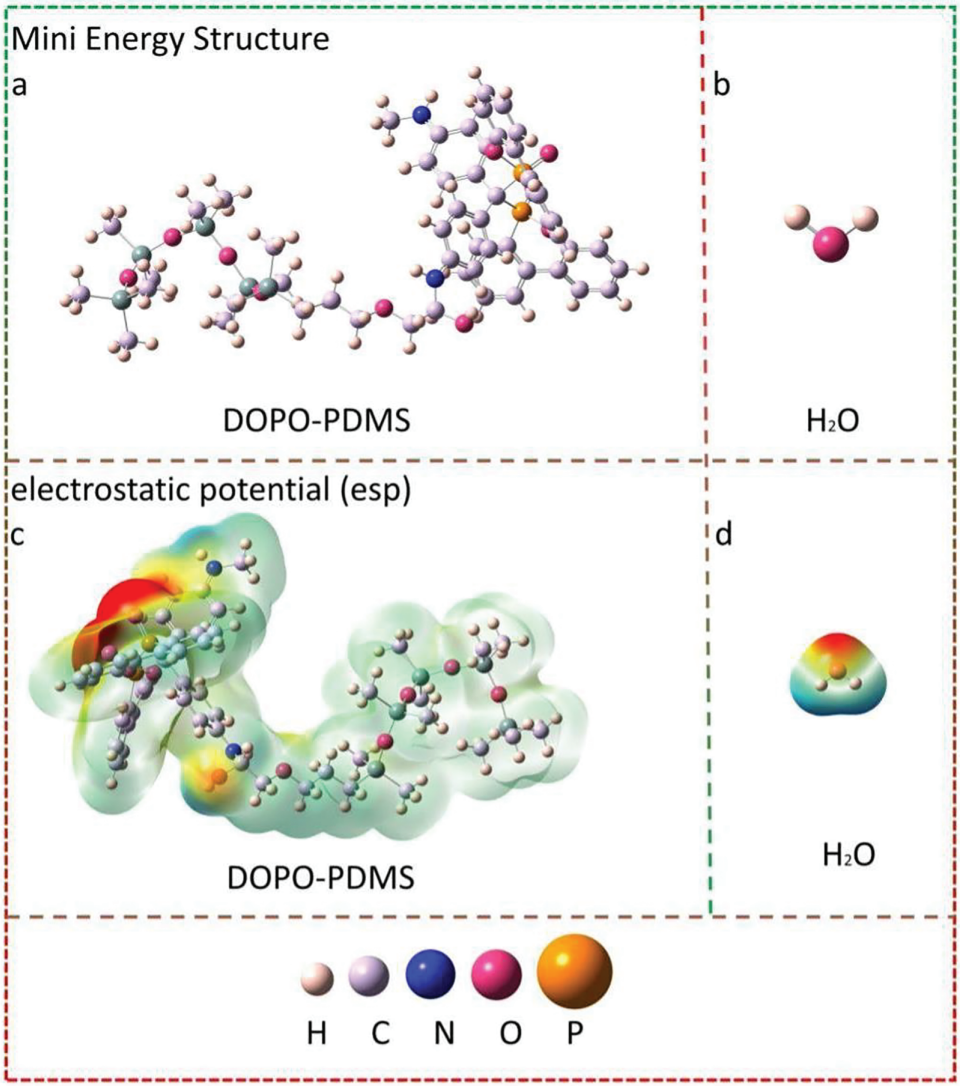

Figure 5: (**a**) Optimized minimum-energy geometry of the DOPO-PDMS structure, (**b**) Optimized minimum-energy geometry of the H_2O molecule, (**c**) Electrostatic potential (ESP) map of DOPO-PDMS, (**d**) Electrostatic potential (ESP) map of H_2O.

For DOPO-NH_2-PDMS, the PDMS segment shows no apparent electron-rich or electron-deficient regions along the chain. In contrast, the EPS of H_2O displays a clear electron-rich region around the oxygen atom and electron-deficient regions near the hydrogen atoms. Such complementary charge distributions typically promote attractive interactions between molecular fragments. Because the PDMS backbone lacks distinct electron-donating or electron-withdrawing regions, there is essentially no electrostatic driving force for H_2O molecules to interact with it. This absence of favorable interactions helps explain the pronounced hydrophobic behavior of the PDMS-containing structure.

The mechanical durability of the coatings was evaluated using pencil hardness and steel-wool abrasion tests (Figs. 6 and 7). As a qualitative study, this experiment assessed the wear resistance by comparing the abrasion degree between the unmodified and modified epoxy coatings under the same conditions, with evaluation criteria including the damaged area and depth. The unmodified epoxy coating could only withstand scratches below 1H hardness without obvious marks, while visible scratches and surface failure (damage reaching the substrate) occurred under higher loads. Incorporation of CEOS–DOPO–PDMS significantly enhanced surface damage resistance: the 5:100 sample could resist scratches up to 2H hardness, whereas the 20:100 coating endured loads up to 5H without visible structural damage (damage remained on the coating surface). After repeated rubbing with steel wool (50 cycles), the unmodified epoxy surface exhibited severe abrasion and loss of gloss (damage reaching the substrate), while the 20:100 NP-GLIDE coating only showed minor surface spots (slight damage on the coating surface) with the overall structure intact.

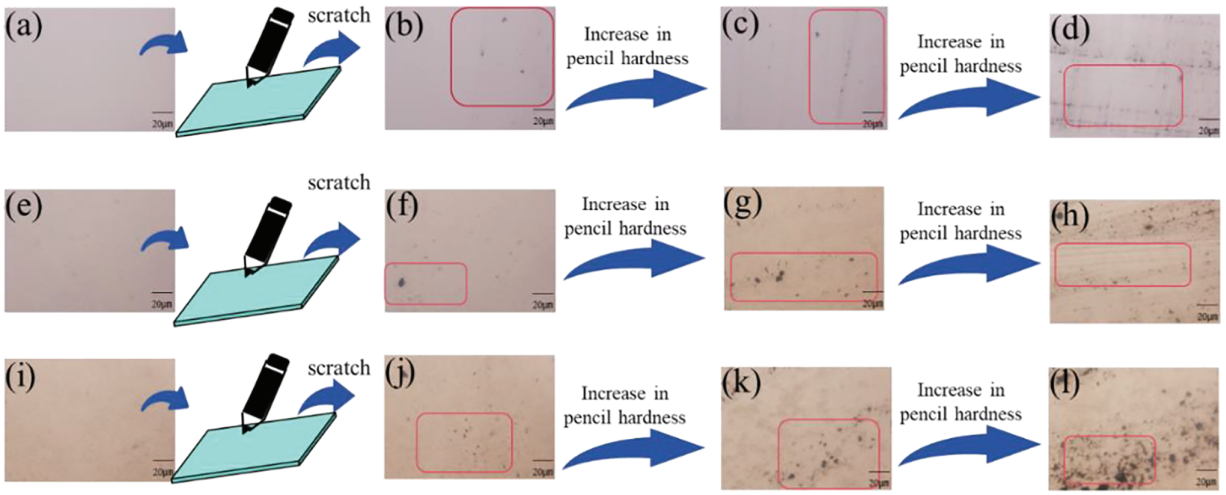

Figure 6: Pencil hardness test results of epoxy-based NP-GLIDE coatings with varying CEOS-DOPO-PDMS content, (**a**–**d**) the blank, 1H, 3H, and 5H test results for the conventional epoxy coating, (**e**–**h**) the blank, 1H, 3H, and 5H test results for the CEOS-DOPO-PDMS:DGEBA = 5:100 coating, (**i**–**l**) the blank, 1H, 3H, and 5H test results for the CEOS-DOPO-PDMS:DGEBA = 20:100 coating.

This enhancement can be ascribed to the formation of a unique organic–inorganic hybrid network during curing, which combines the elasticity of PDMS with the rigidity of CEOS domains. Network density (or crosslink density), conventionally defined as the number of effective chemical crosslinking points per unit volume in thermosetting polymers [46], is a critical parameter influencing mechanical performance and abrasion resistance [47,48]. It should be noted that the stoichiometric ratio of epoxy resin (DGEBA) to curing agent (Jeffamine D230) was kept constant across all formulations in this study. This experimental design was intended to ensure that the chemical crosslink density of the main network formed by the fundamental epoxy-amine reaction remained essentially consistent, thus allowing performance differences to be more clearly attributed to the unique structural effects induced by the additive. As indicated by the experimental results, the coating with a CEOS-DOPO-PDMS:DGEBA mass ratio of 20:100 exhibits significantly superior abrasion resistance compared to the coating with a ratio of 5:100. This phenomenon is primarily attributed to the formation of a more developed and continuous nano-scale hybrid reinforcement network at higher additive dosages, which enhances stress distribution, interfacial adhesion, and resistance to mechanical wear, rather than increasing the chemical crosslink density of the epoxy matrix. Based on this, it can be preliminarily inferred that within the scope of this experimental system, the improvement in the coating's

abrasion resistance is driven by the enhanced physical reinforcement effect of the hybrid structure rather than a simple linear increase in chemical crosslink density. It is noteworthy that PDMS enhances the adhesion of the coating [49,50], so the influence of the adhesion strength between the coating and the substrate on the experimental results can be neglected. The flexible PDMS chains dissipate external stress, while the inorganic Si–O–Si backbone contributes to high hardness and wear resistance. Furthermore, the dense hybrid interface between CEOS-DOPO-PDMS and the epoxy matrix effectively suppresses crack propagation, leading to improved toughness and mechanical durability.

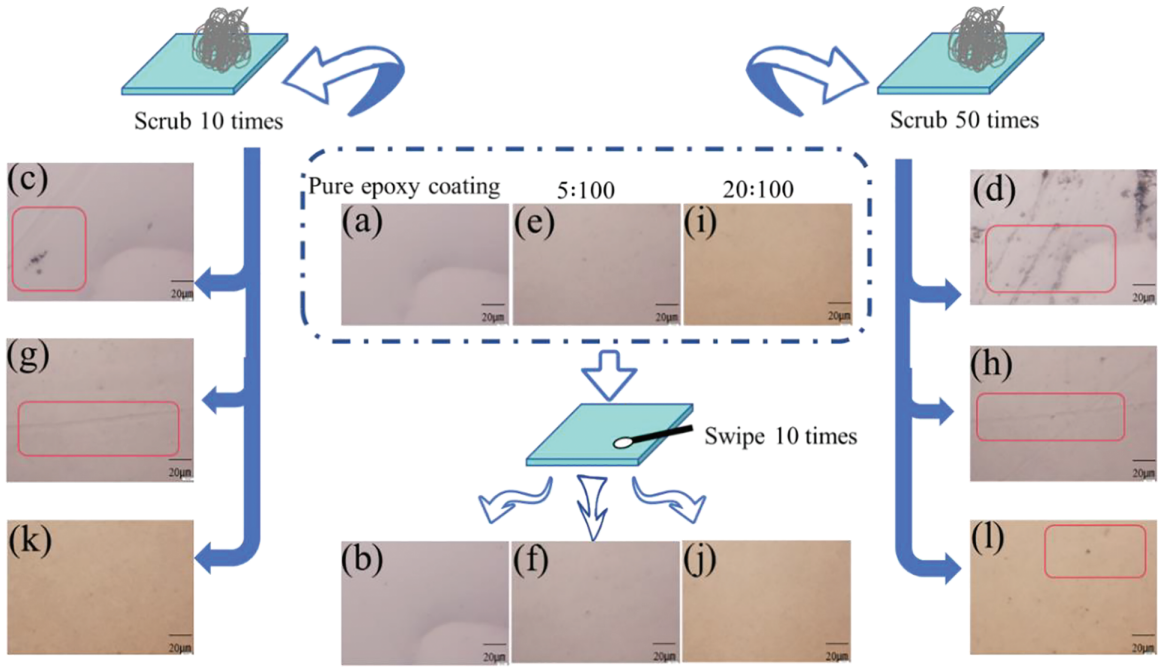

Figure 7: Steel wool abrasion resistance test results of epoxy-based NP-GLIDE coatings with varying CEOS-DOPO-PDMS content (**a**–**d**) the blank, 10-swab abrasion, 10-wire-wool abrasion, and 50-wire-wool abrasion test results for the conventional epoxy coating, (**e**–**h**) the blank, 10-swab abrasion, 10-wire-wool abrasion, and 50-wire-wool abrasion test results for the CEOS-DOPO-PDMS:DGEBA = 5:100 coating, (**i**–**l**) the blank, 10-swab abrasion, 10-wire-wool abrasion, and 50-wire-wool abrasion test results for the CEOS-DOPO-PDMS:DGEBA = 20:100 coating.

3.2.3 Combustion Behavior Evaluation

Combustion behavior was conducted using a butane torch as the flame-generating device to evaluate the high-temperature combustion resistance of epoxy-based NP-GLIDE coatings with different CEOS–DOPO–PDMS loadings. First, the samples were pretreated to ensure the coating was uniformly applied onto glass substrates with a consistent coating amount on each substrate, after complete curing, the samples were fixed on a horizontal test bench to ensure no wrinkles or damage on the coating surface during the test. Subsequently, the flame temperature of the butane torch was adjusted to approximately 500°C, and the torch was fixed using a bracket to maintain a vertical distance of 15 cm between the flame nozzle and the coating surface, ensuring uniform flame exposure on the coating. After igniting the torch, the coating was subjected to targeted combustion for 30 consecutive sec, during combustion, a Uti32 infrared thermal imager (Uni-Trend Technology Co., Ltd., China) was used to real-time record the temperature change curve and dynamic surface morphology evolution of the coating, capturing key phenomena such as melting and carbonization of the coating under flame action. After combustion, the samples were cooled to room temperature, and the flame retardant efficiency was evaluated by combining visual observation

and microscopic characterization to analyze the carbonization degree of the coating (e.g., carbonization area ratio, carbon layer thickness) and the morphology of residual char (e.g., compactness, pore structure, bonding state with the substrate), thereby determining the differences in flame retardant performance among coatings with different loadings. The relevant test results are shown in Fig. 8. The infrared thermal image in Fig. 8a records a maximum surface temperature of about 506.2°C during testing, confirming the uniformity of the combustion environment. The pre-combustion appearances of the three coatings, conventional epoxy (0:100), CEOS–DOPO–PDMS:DGEBA = 5:100, and 20:100, are presented in Fig. 8b–d, while their corresponding post-combustion states are shown in Fig. 8e–g, respectively.

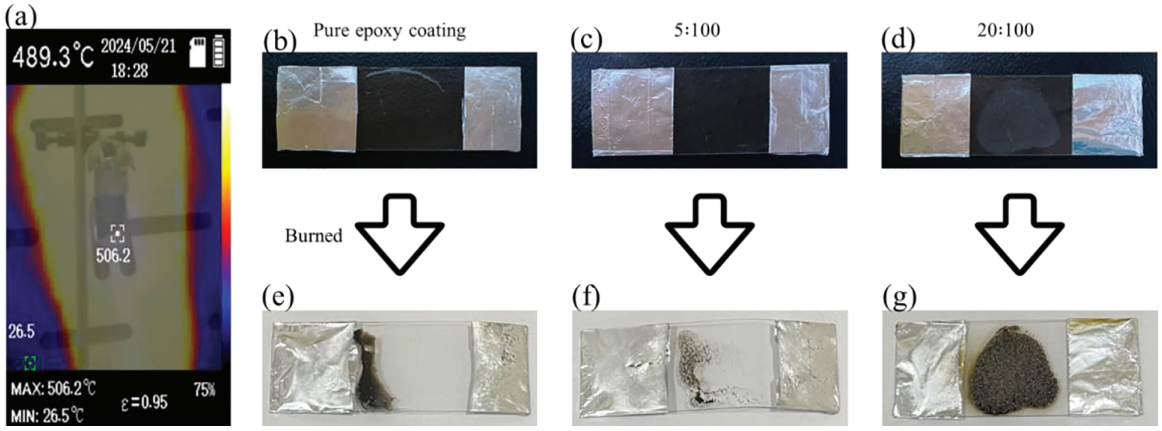

Figure 8: (**a**) Infrared thermal image, (**b**–**d**) the pre-combustion images of the conventional epoxy coating, the CEOS-DOPO-PDMS:DGEBA = 5:100 coating, and the CEOS-DOPO-PDMS:DGEBA = 20:100 coating, respectively, (**e**–**g**) the post-combustion images of the conventional epoxy coating, the CEOS-DOPO-PDMS:DGEBA = 5:100 coating, and the CEOS-DOPO-PDMS:DGEBA = 20:100 coating, respectively.

The conventional epoxy coating (Fig. 8b,e) was almost completely consumed after flame exposure, leaving no coherent residue and displaying extensive charring and material loss, which clearly demonstrates its poor flame resistance. The 5:100 NP-GLIDE coating (Fig. 8c,f) exhibited delayed ignition compared with the control, but most of the coating surface was still degraded after 30 s of combustion. The incomplete residue and irregular surface morphology indicate that the relatively low loading of the flame-retardant hybrid precursor was insufficient to generate a continuous, thermally stable protective layer. In contrast, the 20:100 NP-GLIDE coating (Fig. 8d,g) formed a dense, black, and porous char layer that adhered firmly to the substrate and maintained structural integrity even after prolonged heating. This char morphology reflects the formation of an efficient condensed-phase barrier: phosphorus-containing species derived from DOPO facilitate dehydration while quenching gas-phase radicals, and the CEOS-derived Si–O–Si network reinforces the char, enhancing its cohesion and thermal insulation [51,52].

Overall, Fig. 8a–g clearly illustrates the trend that combustion is significantly reduced with the increase in loading capacity. As the content of CEOS–DOPO–PDMS increases, the high-temperature resistance of the coating is remarkably enhanced while its combustibility is substantially decreased. Thermal imaging results further confirm that the NP-GLIDE coating with a 20:100 ratio maintains a relatively low surface temperature and excellent thermal insulation performance throughout the entire test, highlighting the synergistic effect of the phosphorus-silicon hybrid structure in reducing combustibility.

Comprehensive analysis of the FT-IR, surface morphology, and property evaluations demonstrates that the incorporation of CEOS–DOPO–PDMS leads to a multi-scale hybrid structure in the epoxy NP-GLIDE coating. The micro-rough surface topology combined with the migration of PDMS chains imparts excellent

hydrophobic and self-cleaning behavior. Simultaneously, the presence of rigid Si–O–Si and thermally stable P–O bonds enhances mechanical and flame-retardant properties. These synergistic effects enable the coating to maintain mechanical integrity and thermal protection under extreme conditions, confirming its potential as a multifunctional protective material for advanced engineering applications.

4 Conclusions

A multifunctional epoxy-based NP-GLIDE coating was successfully fabricated through the integration of CEOS–DOPO–PDMS hybrid precursors, achieving simultaneous enhancement of hydrophobicity, wear resistance, and flame retardancy. Structural analyses confirmed the successful synthesis of DOPO-functionalized and siloxane-modified intermediates, and FT-IR results verified the coexistence of P–O, Si–O–Si, and C–O–C linkages within the final cured coating. Optical microscopy revealed a hierarchically rough and porous surface, contributing to its high hydrophobicity with a maximum water contact angle of 109.6°. Mechanical testing demonstrated that the coating sustained scratching up to 5H pencil hardness, indicating excellent surface robustness. In flame-resistance evaluation, the coating maintained structural integrity after exposure to a 500°C flame for 30 s, highlighting the synergistic effect of phosphorus–silicon components in promoting char formation and thermal protection.

The above experiments warrant further improvement. Coating tests were conducted on glass substrates due to their smooth, non-porous, and chemically inert surface, which makes them an ideal choice for controlled laboratory experiments. However, the surface properties of substrates involved in practical applications (e.g., metals, polymers, ceramics, etc.) vary significantly. This can lead to discrepancies in the scratch resistance, durability, or optical properties (such as transparency and reflectivity) of the coating between glass and other materials. For translation to real-world applications, further tests are required, which should involve scaling up the experimental scope to include larger-sized substrates or samples of actual product specifications. This will enable a comprehensive evaluation of the coating's practicality and cost-effectiveness in industrial production.

Overall, the CEOS–DOPO–PDMS-modified epoxy NP-GLIDE coating exhibits a well-balanced combination of surface repellency, mechanical durability, and fire resistance. This work provides an effective strategy for designing high-performance protective coatings with potential applications in architectural materials, electronics, and aerospace engineering. Future studies will focus on optimizing the hybrid network architecture and exploring scalable processing routes to further enhance multifunctional performance and industrial adaptability.

Acknowledgement: This research was supported by the Undergraduate Training Programs for Innovations by NEFU (grant number 202410225370).

Funding Statement: This research was funded by Large-Scale Instrument and Equipment Sharing Service Platform of College of Chemistry, Chemical Engineering and Resource Utilization, NEFU.

Author Contributions: Guoguan Wu: Conceptualization, Methodology, Data curation, Writing—original draft. Baipei Liu: Software, Data curation, Writing—review & editing. Dawei Jiang: Supervision, Project administration, Funding acquisition, Writing—review & editing. Haorui Yu: Investigation, Formal analysis. Jiayu Fu: Methodology, Validation, Visualization. Chengze Yu: Investigation, Resources. Hanbin Wang: Software, Data analysis. Miaojun Xu: Supervision, Writing—review & editing. Zijian Wu: Characterization, Validation. Bin Li: Conceptualization, Supervision, Writing—review & editing. All authors reviewed and approved the final version of the manuscript.

Availability of Data and Materials: The data that support the findings of this study are available from the Corresponding Author, Dawei Jiang, upon reasonable request.

Ethics Approval: Not applicable.

Conflicts of Interest: The authors declare no conflicts of interest.

References

1. Jin FL, Li X, Park SJ. Synthesis and application of epoxy resins: a review. J Ind Eng Chem. 2015;29:1–11. doi:10.1016/j.jiec.2015.03.026.
2. Sreehari H, Sethulekshmi AS, Saritha A. Bio epoxy coatings: an emergent green anticorrosive coating for the future. Macro Mater Eng. 2022;307(8):2200004. doi:10.1002/mame.202200004.
3. Zhang Z, Lu X, Xin Z. Organosilicon-modified epoxy resin coatings for anti-smudge application. J Polym Res. 2025;32(7):224. doi:10.1007/s10965-025-04431-y.
4. Chen Z, Liu X, Chen H, Li J, Wang X, Zhu J. Application of epoxy resin in cultural relics protection. Chin Chemical Lett. 2024;35(4):109194. doi:10.1016/j.cclet.2023.109194.
5. Zhao M, Zhang B, Liu W, Zhang X, Sun M, Zhang X, et al. The effect of polythiol-functionalized molybdenum disulfide nanosheets on the bonding performance of epoxy resin adhesives under different adhesive layer thicknesses. J Appl Polym Sci. 2026;143(3):e58018. doi:10.1002/app.58018.
6. Qian Y, Luo Y, Haruna AY, Xiao B, Li W, Li Y, et al. Multifunctional epoxy-based electronic packaging material MDCF@LDH/EP for electromagnetic wave absorption, thermal management, and flame retardancy. Small. 2022;18(46):2204303. doi:10.1002/smll.202204303.
7. Song P, Ma Z, Qiu H, Ru Y, Gu J. High-efficiency electromagnetic interference shielding of rGO@FeNi/epoxy composites with regular honeycomb structures. Nano Micro Lett. 2022;14(1):51. doi:10.1007/s40820-022-00798-5.
8. Cai R, Huang Z, He R, Bai H, Li J. AC surface flashover and breakdown strength study of boron nitride epoxy resin composite. In: Yang Q, Bie Z, Yang X, editors. Proceedings of the 19th Annual Conference of China Electrotechnical Society; 2024 Sep 20–22; Xi'an, China. Singapore: Springer Nature; 2025. p. 131–9. doi:10.1007/978-981-96-1391-5_15.
9. Nayak SY, Shenoy S, Kini CR, Hameed Sultan MT, Shahar FS. Experimental investigation into mechanical properties of coconut shell powder modified epoxy/3D E-glass composites. Eng Sci. 2022;20:306–20. doi:10.30919/es8e759.
10. Prusov E, Shabaldin I, Lisyatnikov M, Chibrikin D, Roshchina S. Synthesis and properties of polymer composite materials based on epoxy resin with silicon carbide. In: Vatin N, Roschina S, Dixit S, editors. Proceedings of the MPCPE 2024; 2024 Apr 23–25; Vladimir, Russia. Cham, Switzerland: Springer Nature; 2025. p. 261–6. doi:10.1007/978-3-031-81635-2_25.
11. Jing X, Wei J, Liu Y, Song B, Liu Y. Deployment analysis of aramid fiber reinforced shape-memory epoxy resin composites. Eng Sci. 2020;11:44–53. doi:10.30919/es8d1120.
12. Shi K, Shen Y, Zhang Y, Wang T. A modified imidazole as a novel latent curing agent with toughening effect for epoxy. Eng Sci. 2018;5:66–72. doi:10.30919/es8d639.
13. Rawat RS, Talwar M, Diwan RK, Tyagi AK. A study on flame-retardancy property of UV curable epoxy coating for wooden surfaces using boron diluent and phosphorus based initiator. J Polym Mater. 2022;38(3–4):281–94. doi:10.32381/jpm.2021.38.3-4.9.
14. Howell BA. Flame retardants of the future: biobased, organophosphorus, reactive or oligomeric. Front Chem. 2024;12:1500782. doi:10.3389/fchem.2024.1500782.
15. Liu J, Dai J, Wang S, Peng Y, Cao L, Liu X. Facile synthesis of bio-based reactive flame retardant from vanillin and guaiacol for epoxy resin. Compos Part B Eng. 2020;190:107926. doi:10.1016/j.compositesb.2020.107926.
16. Nabipour H, Wang X, Batool S, Song L, Hu Y. A phosphaphenanthrene-containing vanillin derivative as co-curing agent for flame-retardant and antibacterial epoxy thermoset. Polymer. 2021;217:123460. doi:10.1016/j.polymer.2021.123460.
17. Salmeia KA, Gaan S. An overview of some recent advances in DOPO-derivatives: chemistry and flame retardant applications. Polym Degrad Stab. 2015;113:119–34. doi:10.1016/j.polymdegradstab.2014.12.014.

18. Howell BA. Thermal degradation of organophosphorus flame retardants. Polymers. 2022;14(22):4929. doi:10.3390/polym14224929.
19. Qin C, Chen J, Ruan S, Liu F, Zhang L. Theoretical study on the effect of oxidation states of phosphorus flame retardants on their mode of action. Polym Degrad Stab. 2024;223:110735. doi:10.1016/j.polymdegradstab.2024.110735.
20. Yu D, Liu W, Liu Y. Synthesis, thermal properties, and flame retardance of phosphorus-containing epoxy-silica hybrid resins. Polym Compos. 2010;31(2):334–9. doi:10.1002/pc.20809.
21. Ding J, Tao Z, Zuo X, Fan L, Yang S. Preparation and properties of halogen-free flame retardant epoxy resins with phosphorus-containing siloxanes. Polym Bull. 2009;62(6):829–41. doi:10.1007/s00289-009-0052-0.
22. Chen Z, He X, Cao Z, Li Y, Chen D, Yang Z, et al. Syringaldehyde-DOPO derivative for enhancing flame retardancy and mechanical properties of epoxy resin. Fire Mater. 2024;48(7):752–64. doi:10.1002/fam.3228.
23. Zhang YC, Xu GL, Liang Y, Yang J, Hu J. Preparation of flame retarded epoxy resins containing DOPO group. Thermochim Acta. 2016;643:33–40. doi:10.1016/j.tca.2016.09.015.
24. Han Y, Liu Y, Elsharkawy ER, El-Bahy SM, Jiang D, Wu Z, et al. Exploring NP-GLIDE coatings: a leap forward in the innovation of omniphobic surfaces. React Funct Polym. 2024;205:106050. doi:10.1016/j.reactfunctpolym.2024.106050.
25. Lei Y, Han Y, Cheng X, Chen C, Liu B, Xu M, et al. Hydrogen-bond network reconstruction driven transparent α-chitin polyurethane coatings for eco-friendly surface protection: synergistic antifouling and anticorrosion enhancement. Prog Org Coat. 2026;210:109639. doi:10.1016/j.porgcoat.2025.109639.
26. Lai Z, Liu G. Facile preparation of a transparent and rollable omniphobic coating with exceptional hardness and wear resistance. ACS Appl Mater Interfaces. 2022;14(30):35138–47. doi:10.1021/acsami.2c10200.
27. Hu H, Liu G, Wang J. Preparation and comparison of NP-GLIDE, SLIPS, superhydrophobic, and other coatings from identical precursors at different mixing ratios. J Mater Chem A. 2019;7(4):1519–28. doi:10.1039/c8ta11115d.
28. Hu H, Wang J, Wang Y, Gee E, Liu G. Silicone-infused antismudge nanocoatings. ACS Appl Mater Interfaces. 2017;9(10):9029–37. doi:10.1021/acsami.7b00126.
29. Zheng C, Liu G, Hu H. UV-curable antismudge coatings. ACS Appl Mater Interfaces. 2017;9(30):25623–30. doi:10.1021/acsami.7b05732.
30. Hu H, Liu G, Wang J. Clear and durable epoxy coatings that exhibit dynamic omniphobicity. Adv Mater Inter. 2016;3(14):1600001. doi:10.1002/admi.201600001.
31. Khan F, Rabnawaz M, Li Z, Khan A, Naveed M, Tuhin MO, et al. Simple design for durable and clear self-cleaning coatings. ACS Appl Polym Mater. 2019;1(10):2659–67. doi:10.1021/acsapm.9b00596.
32. Choi WT, Kim DW, Jeong YT, Hong SS, Gal YS, Lim KT. Preparation of colorless polyimide hybrid films with enhanced optical, chemical and thermal resistance. Mol Cryst Liq Cryst. 2019;679(1):87–94. doi:10.1080/15421406.2019.1597550.
33. Wang X, He W, Long L, Huang S, Qin S, Xu G. A phosphorus- and nitrogen-containing DOPO derivative as flame retardant for polylactic acid (PLA). J Therm Anal Calorim. 2021;145(2):331–43. doi:10.1007/s10973-020-09688-7.
34. Wu CS, Liu YL, Chiu YS. Synthesis and characterization of new organosoluble polyaspartimides containing phosphorus. Polymer. 2002;43(6):1773–9. doi:10.1016/s0032-3861(01)00751-0.
35. Yang S, Kim JS, Jin J, Kwak SY, Bae BS. Cycloaliphatic epoxy oligosiloxane-derived hybrid materials for a high-refractive index LED encapsulant. J Appl Polym Sci. 2011;122(4):2478–85. doi:10.1002/app.34375.
36. Kartsev DD, Prilepskii AY, Lukyanov IM, Sharapenkov EG, Klaving AV, Goltaev A, et al. Fabrication of omniphobic-omniphilic micropatterns using GPOSS-PDMS coating. Adv Mater Inter. 2023;10(16):2300156. doi:10.1002/admi.202300156.
37. Chu HH, Chen YL, Shen BH, Chuang KS. Epoxy/nanosilica organic-inorganic hybrid materials-effect of functional group of POSS. Fibres Polym. 2022;23(10):2927–36. doi:10.1007/s12221-022-4016-4.
38. Odagiri N, Shirasu K, Kawagoe Y, Kikugawa G, Oya Y, Kishimoto N, et al. Amine/epoxy stoichiometric ratio dependence of crosslinked structure and ductility inamine-curedepoxy thermosetting resins. J Appl Polym Sci. 2021;138(23):50542. doi:10.1002/app.50542.

39. Frisch M, Trucks G, Schlegel H, Scuseria G, Robb M, Cheeseman J, et al. Gaussian 16 Rev. C. 01. Wallingford, CT, USA: Gaussian, Inc.; 2016.
40. Miehlich B, Savin A, Stoll H, Preuss H. Results obtained with the correlation energy density functionals of becke and Lee, Yang and Parr. Chem Phys Lett. 1989;157(3):200–6. doi:10.1016/0009-2614(89)87234-3.
41. Lee C, Yang W, Parr RG. Development of the Colle-Salvetti correlation-energy formula into a functional of the electron density. Phys Rev B. 1988;37(2):785–9. doi:10.1103/physrevb.37.785.
42. Krishnan R, Binkley JS, Seeger R, Pople JA. Self-consistent molecular orbital methods. XX. A basis set for correlated wave functions. J Chem Phys. 1980;72(1):650–4. doi:10.1063/1.438955.
43. Frisch MJ, Pople JA, Binkley JS. Self-consistent molecular orbital methods 25. Supplementary functions for Gaussian basis sets. J Chem Phys. 1984;80(7):3265–9. doi:10.1063/1.447079.
44. Stanton MM, Ducker RE, MacDonald JC, Lambert CR, McGimpsey WG. Super-hydrophobic, highly adhesive, polydimethylsiloxane (PDMS) surfaces. J Colloid Interface Sci. 2012;367(1):502–8. doi:10.1016/j.jcis.2011.07.053.
45. Santiago AAG, Gondim JGS, Tranquilin RL, Silva FS, Fernandez FF, Costa MCB, et al. Development of ZnO/PDMS nanocomposite with photocatalytic/hydrophobic multifunction. Chem Phys Lett. 2020;740:137051. doi:10.1016/j.cplett.2019.137051.
46. Vernerey FJ, Brighenti R, Long R, Shen T. Statistical damage mechanics of polymer networks. Macromolecules. 2018;51(17):6609–22. doi:10.1021/acs.macromol.8b01052.
47. Molero G, Sue HJ. Scratch behavior of model epoxy resins with different crosslinking densities. Mater Des. 2019;182:107965. doi:10.1016/j.matdes.2019.107965.
48. Kim B, Choi J, Yang S, Yu S, Cho M. Influence of crosslink density on the interfacial characteristics of epoxy nanocomposites. Polymer. 2015;60:186–97. doi:10.1016/j.polymer.2015.01.043.
49. Liu J, Jiang Z, Li Y, Kang G, Qu S. Stability of hydrogel adhesion enabled by siloxane bonds. Eng Fract Mech. 2022;271:108662. doi:10.1016/j.engfracmech.2022.108662.
50. Kroner E, Paretkar DR, McMeeking RM, Arzt E. Adhesion of flat and structured PDMS samples to spherical and flat probes: a comparative study. J Adhes. 2011;87(5):447–65. doi:10.1080/00218464.2011.575317.
51. Bifulco A, Varganici CD, Rosu L, Mustata F, Rosu D, Gaan S. Recent advances in flame retardant epoxy systems containing non-reactive DOPO based phosphorus additives. Polym Degrad Stab. 2022;200:109962. doi:10.1016/j.polymdegradstab.2022.109962.
52. Yang Y, Wang DY, Jian RK, Liu Z, Huang G. Chemical structure construction of DOPO-containing compounds for flame retardancy of epoxy resin: a review. Prog Org Coat. 2023;175:107316. doi:10.1016/j.porgcoat.2022.107316.